

Testing non-standard neutrino interactions in (anti)-electron neutrino disappearance experiments

M. E. Chaves, P. C. de Holanda, and O. L. G. Peres

Instituto de Física Gleb Wataghin - UNICAMP, 13083-859, Campinas SP, Brazil

E-mail: mchaves@ifi.unicamp.br, [ORCID:0000-0001-7396-081X](https://orcid.org/0000-0001-7396-081X),

holanda@ifi.unicamp.br, [ORCID: 0000-0001-9852-8900](https://orcid.org/0000-0001-9852-8900),

orlando@ifi.unicamp.br, [ORCID:0000-0003-2104-8460](https://orcid.org/0000-0003-2104-8460)

ABSTRACT: We search for scalar and tensor non-standard interactions using (anti)-electron neutrino disappearance in oscillation data. We found a slight preference for non-zero CP violation, coming from both tensor and scalar interactions. The preference for CP violation is lead by Daya Bay low-energy data with a significance that reaches $\sim 1.7\sigma$ in the global analysis (and $\sim 2.1\sigma$ when considering only medium baseline reactors data) compared to the standard oscillation scenario.

Contents

1	Introduction	1
2	BSM physics effects on neutrino oscillation	2
2.1	Neutrino oscillations in reactors	4
2.1.1	Reactors neutrino production and detection factors	5
2.2	Flavour conversion in the sun	7
2.2.1	Solar neutrino production and detection factors	9
3	Analysis details	9
3.1	Medium baseline reactors	9
3.2	KamLand experiment	10
3.3	Solar experiments	11
3.4	Global picture	11
4	Results	12
4.1	The $[\tilde{\epsilon}_X]_{e\tau}$ analysis	12
4.2	The $[\tilde{\epsilon}_X]_{e\mu}$ analysis	13
4.3	CP violation	16
5	Conclusions	17
A	Analytical expressions	22
B	Rephasing invariants with non-standard neutrino interaction	23
C	Solar+KamLand analysis	24

1 Introduction

Since the establishment of the neutrino flavour oscillations [1, 2], the effect was consistently probed by several experiments [3–17]. In the present scenario, there are six measured parameters: θ_{13} , θ_{12} , θ_{23} , Δm_{21}^2 and Δm_{3i}^2 [18]. Remains unknown, the CP violation phase and the mass-hierarchy, which can be determined in the next few decades by Hyper-Kamiokande [19], DUNE [20], and JUNO [21]. The neutrino oscillation experiments offer a new opportunity to search for effects of new physics coming from the neutrino sector, e.g, neutrino decays [22–24] and non-standard neutrino interactions (NSI) [25–35].

The NSI can be classified according to its effects on experiments: as interactions in the production and detection (charged current) or interactions in the propagation (neutral current). Regarding neutrino interactions in the production and detection, it's frequent

the search for left-handed interactions [36–46] except for some recent works in the context of SMEFT [47, 48].

In this work, we search for scalar and tensor interactions in the (anti)-neutrinos production (and detection) for reactors [3–6] and solar [10–17] experiments. The scalar and tensor interactions provide a new source of CP violation that is not present in the standard oscillation scenario for the (anti)-neutrino disappearance. The Lagrangian considered in this work is:

$$\begin{aligned} \mathcal{L} = & -2\sqrt{2}G_F V_{ud} \{ (\bar{u}\gamma^\mu P_L d)(\bar{\ell}_\alpha \gamma_\mu P_L \nu_\alpha) + \frac{1}{2}[\epsilon_S]_{\alpha\beta}(\bar{u}d)(\bar{\ell}_\alpha P_L \nu_\beta) \\ & + \frac{1}{4}[\epsilon_T]_{\alpha\beta}(\bar{u}\sigma^{\mu\nu} P_L d)(\bar{\ell}_\alpha \sigma_{\mu\nu} P_L \nu_\beta) + \text{h.c.} \} , \end{aligned} \quad (1.1)$$

where the first term is the usual Standard Model Lagrangian, the second (third term) is the scalar (tensorial) coupling proportional to the scalar (tensorial) relative coupling $[\epsilon_S]_{\alpha\beta}([\epsilon_T]_{\alpha\beta})$. We normalized the BSM terms by the the Fermi coupling constant G_F , and V_{ud} is a CKM matrix element. The tensorial structure is given by $\sigma^{\mu\nu} = i[\gamma^\mu, \gamma^\nu]/2$, and $P_{L,R}$ are the chirality projectors $(1 \mp \gamma_5)/2$.

The article is organized as follows, in Sec. 2, we introduce the formalism used in this work and extend the analysis of [47] to include non-linear terms, the Δm_{31}^2 and the solar parameters θ_{12} and Δm_{21}^2 . In Sec. 3 we present the details of our analysis and in Sec. 4 our results.

2 BSM physics effects on neutrino oscillation

The effects of the BSM physics in the detection and production of the neutrinos was computed following the Reference [45, 47]. We first compute the rate for a ν_α being produced and a ν_β being detected in the Standard Model

$$R_{\alpha\beta}^{\text{SM}} \propto \sum_{k,l} \int d\Pi_P d\Pi_D (\mathcal{M}_{\alpha k}^P)^{\text{SM}} (\overline{\mathcal{M}}_{\alpha l}^P)^{\text{SM}} (\mathcal{M}_{\beta k}^D)^{\text{SM}} (\overline{\mathcal{M}}_{\beta l}^D)^{\text{SM}} = \phi_\alpha^{\text{SM}} \sigma_\beta^{\text{SM}} \quad (2.1)$$

where $(\mathcal{M}_{\alpha k}^{P,D})^{\text{SM}}$ are the amplitudes for production of a ν_α neutrino and the detection of a ν_β neutrino in the Standard Model, ϕ_α^{SM} is the ν_α neutrino flux and σ_β^{SM} the detection cross-section for ν_β neutrino. Notice that there is no dependence of distance between the source and of the detection of neutrino. Similarly the rates with BSM physics for a neutrino produced as ν_α state, having travelled a distance L and detected as ν_β state is

$$R_{\alpha\beta} \propto \sum_{k,l} e^{-iL\phi_{kl}} \int d\Pi_P d\Pi_D \mathcal{M}_{\alpha k}^P \overline{\mathcal{M}}_{\alpha l}^P \mathcal{M}_{\beta k}^D \overline{\mathcal{M}}_{\beta l}^D, \quad (2.2)$$

where $\mathcal{M}_{\alpha k}^P(\mathcal{M}_{\beta k}^D)$ is the production, P (detection, D), amplitude for $\nu_\alpha(\nu_\beta)$ for the BSM physics after the neutrino has travelled a distance L . Here, $\phi_{kl} \equiv \Delta m_{kl}^2/2E_\nu$, with $\Delta m_{kl}^2 \equiv m_k^2 - m_l^2$ is the mass difference between the mass eigenstates k and l , and E_ν is the neutrino energy.

We can write the production amplitude of BSM physics as

$$\mathcal{M}_{\alpha k}^P = U_{\alpha i} \mathcal{M}_{\text{SM}}^P + [\epsilon_X U]_{\alpha i} \mathcal{M}_X^P \quad (2.3)$$

here, $U_{\alpha l}$ are components of the PMNS matrix [49, 50] that rotates the neutrino flavor fields into neutrino mass fields. Similarly for the detection amplitude $\mathcal{M}_{\alpha k}^D$, replacing $U_{\alpha i} \mathcal{M}_{\text{SM}}^P \rightarrow U_{\alpha i}^* \mathcal{M}_{\text{SM}}^D$ and $[\epsilon_X U]_{\alpha i} \mathcal{M}_X^P \rightarrow [\epsilon_X U]_{\alpha i}^* \mathcal{M}_X^D$.

The relative change of the rate with BSM physics for a ν_α being produced and ν_β being detected, replacing eq. (2.3) into eq. (2.2) and using eq. (2.1) we got

$$\frac{R_{\alpha\beta}}{\phi_\alpha^{\text{SM}} \sigma_\beta^{\text{SM}}} = \sum_{k,l} e^{-i\phi_{kl}L} \left[V_\alpha^{kl}(p_X) \right] \times \left[V_\beta^{kl}(d_X) \right]^*. \quad (2.4)$$

where

$$V_\alpha^{kl}(p_X) = U_{\alpha k}^* U_{\alpha l} + p_{XL} (\epsilon_X U)_{\alpha k}^* U_{\alpha l} + p_{XL}^* U_{\alpha k} (\epsilon_X U)_{\alpha l} + p_{XX} (\epsilon_X U)_{\alpha k}^* (\epsilon_X U)_{\alpha l}, \quad (2.5)$$

and $p_{XY}(d_{XY})$ is the ratio of the production (detection) interference amplitude term $\mathcal{M}_{\alpha k}^X$ with $\mathcal{M}_{\alpha k}^Y$ over the SM amplitude. The interaction can be the standard model, scalar or tensorial ($X = \{SM, S, T\}$) as given in eq. (1.1). We will call in this article as *neutrino production and detection factors*. They are

$$p_{XY} \equiv \frac{\int d\Pi_P A_X^P \bar{A}_Y^P}{\int d\Pi_P |A_{\text{SM}}^P|^2}, \quad d_{XY} \equiv \frac{\int d\Pi_D A_X^D \bar{A}_Y^D}{\int d\Pi_D |A_{\text{SM}}^D|^2}, \quad (2.6)$$

The expression for anti-neutrinos is replacing in eq. (2.4),

$$U \rightarrow U^* \quad [\epsilon_X]_{\alpha\beta} \rightarrow [\epsilon_X]_{\alpha\beta}^* \quad (2.7)$$

The rate for NSI computed, see eq. (2.6), is the main difference between the usual assumption in the literature that the NSIpd couplings are constant. The departure of the coefficients p_{XL} and p_{XL} from unity, and in special that they are energy dependent, this behaviour can be tested in neutrino experiments.

When turned off the BSM Lagrangian the eq. (2.4), $[\epsilon_X]_{\alpha\beta} \rightarrow 0$, we return to expression of the usual neutrino conversion probability for a initial neutrino ν_α to a final neutrino (ν_β). For non-zero BSM couplings, we can understand the right side of Eq. (2.4) as effective probabilities [45, 47]. We caution the reader that this effective probabilities have non-unitary behaviour.

We will assume a particular PMNS parametrization that is very convenient for studying the behaviour when we have (anti)-electron neutrino as initial and final states. The quantity $V_\alpha^{kl}(p_X)$, defined in Eq. (2.5) will depend on the PMNS matrix U and the BSM coupling $[\epsilon_X]_{\alpha\beta}$. We will use, in this work, an alternative parametrization of PMNS matrix, defined by

$$U_{\text{PMNS}} = U(\theta_{23}, \delta) R(\theta_{13}) R(\theta_{12}) \quad (2.8)$$

where

$$U(\theta_{23}, \delta) = \begin{pmatrix} 1 & 0 & 0 \\ 0 & c_{23} & s_{23}e^{i\delta} \\ 0 & -s_{23}e^{-i\delta} & c_{23} \end{pmatrix}, \quad R_{13} = \begin{pmatrix} c_{13} & 0 & s_{13} \\ 0 & 1 & 0 \\ -s_{13} & 0 & c_{13} \end{pmatrix}, \quad R_{12} = \begin{pmatrix} c_{12} & s_{12} & 0 \\ -s_{12} & c_{12} & 0 \\ 0 & 0 & 1 \end{pmatrix}, \quad (2.9)$$

where $c_{ij} \equiv \cos \theta_{ij}$, $s_{ij} \equiv \sin \theta_{ij}$ for $i, j=1, 2, 3$. This parametrization is also used in the reference [51]. The usual PMNS parametrization is $U_{\text{PMNS}} = R(\theta_{23})U(\theta_{13}, \delta)R(\theta_{12})$ that we can get from Eq. (2.9) changing $U(\theta_{23}, \delta) \rightarrow R(\theta_{23})$ and $R_{13} \rightarrow U(\theta_{23}, \delta)$. Using the Eq. (2.8) to write down

$$(\epsilon_X U) \equiv [\epsilon_X]U = [\epsilon_X]U(\theta_{23}, \delta)R(\theta_{13})R(\theta_{12}) = [\tilde{\epsilon}_X]R(\theta_{13})R(\theta_{12}), \quad (2.10)$$

where we define the effective BSM parameter,

$$[\tilde{\epsilon}_X] \equiv [\epsilon_X]U(\theta_{23}, \delta), \quad (2.11)$$

where

$$\begin{aligned} [\tilde{\epsilon}_X]_{e\mu} &= c_{23}[\epsilon_X]_{e\mu} - s_{23}[\epsilon_X]_{e\tau}e^{-i\delta}, \\ [\tilde{\epsilon}_X]_{e\tau} &= c_{23}[\epsilon_X]_{e\mu}e^{i\delta} + s_{23}[\epsilon_X]_{e\tau}, \end{aligned}$$

the BSM effective coupling $(\epsilon_X U)$ can be computed for initial and final electron-neutrinos as

$$(\tilde{\epsilon}_X O_{13} O_{12})_{e1} = -(s_{12}[\tilde{\epsilon}_X]_{e\mu} + c_{12}s_{13}[\tilde{\epsilon}_X]_{e\tau}), \quad (2.12)$$

$$(\tilde{\epsilon}_X O_{13} O_{12})_{e2} = +(c_{12}[\tilde{\epsilon}_X]_{e\mu} - s_{12}s_{13}[\tilde{\epsilon}_X]_{e\tau}), \quad (2.13)$$

$$(\tilde{\epsilon}_X O_{13} O_{12})_{e3} = c_{13}[\tilde{\epsilon}_X]_{e\tau}. \quad (2.14)$$

Then, *the relevant parameters for our analysis* are the mixing angles and mass differences $\theta_{12}, \theta_{13}, \Delta m_{31}^2, \Delta m_{21}^2$ and real and imaginary part of BSM effective coupling, $[\tilde{\epsilon}_X]$. We graphically displayed this information in Figure (1), for experiments used in this analysis, Daya Bay, RENO, Double Chooz, and KamLand and the solar experiments and connecting by solid (dashed) lines the parameters more (less) relevant for a given experiment. There is an unusual sensitivity in reactors experiment Daya Bay (DB), RENO, and Double Chooz (DC) to Δm_{21}^2 oscillations come from the CP violation effect of the $[\tilde{\epsilon}_X]_{e\mu}$ parameter. The advantage to use the specific PMNS parametrization (2.8) is now evident due all information on the mixing angle θ_{23} the CP phase δ and BSM coupling $[\epsilon_S]$ it is encoded in the effective BSM coupling $[\tilde{\epsilon}_X]$. As can be seen from Eqs. (2.12), (2.13) and (2.12), $[\tilde{\epsilon}_X]_{\mu\tau}$ and the diagonals $[\tilde{\epsilon}_X]_{\mu\mu}$ and $[\tilde{\epsilon}_X]_{\tau\tau}$ does not appear in the final expression for the electron neutrino disappearance. The $[\epsilon_X]_{ee}$ will not be considered here, given the constraints imposed by inverse beta decay, see Ref. [47].

2.1 Neutrino oscillations in reactors

For reactors we have anti-electron neutrinos in the process, then we should use Eq. (2.7) into in Eq. (2.4) to get the anti-electron expression. We will rewrite the BSM rate in a

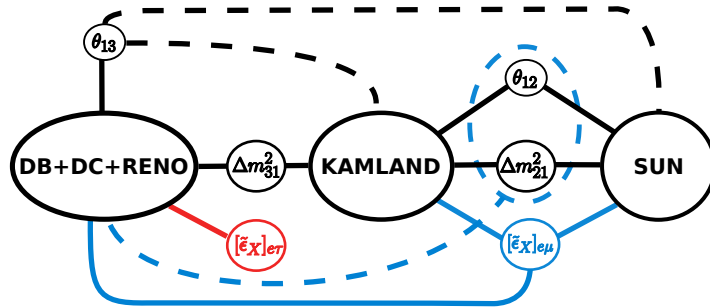


Figure 1. The solid (dashed) lines connect the relevant (less relevant) parameters to each experiment, Daya Bay (DB) [5], RENO [6], Double Chooz (DC) [4], KamLand [3] and solar experiments (SUN).

more appealing structure separating non-oscillation, oscillations, and CP violation terms, for $\alpha = \beta = \bar{e}$,

$$\frac{R_{ee}}{\phi_e^{\text{SM}} \sigma_e^{\text{SM}}} = N^{\text{non-osc}} - \sum_{k>l} N_{kl}^{\text{osc}} \sin^2 \left(\frac{\phi_{kl} L}{2} \right) + \sum_{k>l} N_{kl}^{\text{CP}} \sin(\phi_{kl} L), \quad (2.15)$$

here, the $N^{\text{non-osc}}$ is the term responsible for the zero distance effect [36–46], where even for $L \rightarrow 0$ we will have non-zero effect of the BSM physics and it is a consequence of the non-unitary behaviour of BSM rate. For standard oscillations we have $N^{\text{non-osc}} = 1$. The other terms are the N_{kl}^{osc} and N_{kl}^{CP} , the former are the amplitudes of oscillation, the latter are the amplitudes for the CP violation terms generated by the interference of the standard model amplitudes with the new interactions. The full expressions for the amplitudes, for the relevant case $\alpha = \beta = e$ can be found in the Appendix A.

2.1.1 Reactors neutrino production and detection factors

As commented before, in this formalism we compute the production and detection

In reactors, we assume that anti-neutrinos are produced mainly from Gamow-Teller decays and the detection of comes from inverse beta process (Gamow-Teller and Fermi).

$$\begin{aligned} \beta^- : {}^A_Z N_i &\rightarrow {}^A_{Z+1} N_f + e^- + \bar{\nu}_e, & (\text{production}) \\ \text{inv. } \beta^+ : {}^A_Z N_i + \bar{\nu}_e &\rightarrow e^+ + {}^A_{Z-1} N_f, & (\text{detection}) \end{aligned} \quad (2.16)$$

For our calculations, we use the Lagrangian of Eqs. (1.1) and compute the factors p_{XL} and d_{XL} given in eq. (2.6) for scalar and tensorial interactions. The results are in Table (1) are *energy dependent and this is a distinct behaviour of this formalism*. The p_{XL} and d_{XL} coefficients are functions of the positron energy and the neutrino energy. For low-energy, the positron energy can related to the neutrino electron by the relation $E_e = E_\nu - \Delta_{fi}$, where $\Delta_{fi} = m_{N_f} - m_{N_i}$ is the mass difference between the final and initial nucleon.

Each of neutrino experiments that we are going to test have a different sensitivity to the two mass difference present in PMNS scenario, Δm_{31}^2 and Δm_{21}^2 . In Daya Bay (DB) [5], RENO [6] and Double Chooz (DC) [4] experiments that are medium baseline experiments

	scalar	tensor		scalar	tensor
p_{XL}	0	$-\frac{g_T}{g_A} \frac{m_e}{f(E_\nu)}$	p_{XX}	$\frac{g_S^2}{3g_A^2}$	$\frac{g_T^2}{g_A^2}$
d_{XL}	$\frac{g_S g_V}{g_V^2 + 3g_A^2} \frac{m_e}{E_e}$	$\frac{3g_A g_T}{g_V^2 + 3g_A^2} \frac{m_e}{E_e}$	d_{XX}	$\frac{g_S^2}{g_V^2 + 3g_A^2}$	$\frac{3g_T^2}{g_V^2 + 3g_A^2}$

Table 1. Production and detection factors, Eq. (2.6) for reactors neutrinos. Here E_e is the positron energy, m_e is the electron mass and $f(E_\nu)$ take in to account the nuclear fuel [47] and sub-products in the reactor model, and the g_A , g_T and g_S were extracted from Refs. [52–54].

with $\frac{L}{E_\nu} \sim \frac{1\text{km}}{3\text{MeV}}$, the product $\phi_{kl}L$ that appear in Eq. (2.2) can be written as

$$\phi_{31}L = 4.3 \left(\frac{\Delta m_{31}^2}{2.4 \times 10^{-3}\text{eV}^2} \right) \left(\frac{L}{1000\text{m}} \right) \left(\frac{3\text{MeV}}{E} \right) \quad \phi_{21}L \ll 10^{-2} \left(\frac{L}{1000\text{m}} \right) \quad (2.17)$$

With these results the contribution to the the oscillation, due the $\sin^2(\phi_{kl}L)$ function only the Δm_{31}^2 contribution is relevant. When we have BSM physics, for the medium baseline the N_{kl}^{osc} term will be proportional to $(\tilde{\epsilon}_X O_{13} O_{12})_{e3}$ given in Eq. (2.14), thereafter, proportional to $[\tilde{\epsilon}_X]_{e\tau}$:

$$N_{\text{atm}}^{\text{osc}} = s_{2\theta_{13}}^2 + 2s_{2\theta_{13}}c_{2\theta_{13}} \text{Re}\{[\tilde{\epsilon}_X]_{e\tau}\} (d_{XL} + p_{XL}) + \mathcal{O}([\tilde{\epsilon}_X]_{e\alpha}^2) \quad (2.18)$$

where we define $s_{2\theta_{ij}} \equiv \sin(2\theta_{ij})$, $c_{2\theta_{ij}} \equiv \cos(2\theta_{ij})$. This result implies that these experiments can only test $[\tilde{\epsilon}_X]_{e\tau}$, but not the $[\tilde{\epsilon}_X]_{e\mu}$. For KamLand [3], the more relevant oscillation scale it is $\phi_{21}L = 5.8 \left(\frac{\Delta m_{21}^2}{7.5 \times 10^{-5}\text{eV}^2} \right) \left(\frac{L}{180\text{km}} \right) \left(\frac{3\text{MeV}}{E} \right)$. The $N_{\text{sun}}^{\text{osc}}$ contribution for this experiment is

$$N_{\text{sun}}^{\text{osc}} = c_{13}^3 s_{2\theta_{12}}^2 (c_{13} + 2(t_{2\theta_{12}} \text{Re}\{[\tilde{\epsilon}_X]_{e\mu}\} + s_{13} \text{Re}\{[\tilde{\epsilon}_X]_{e\tau}\}) (d_{XL} + p_{XL}) + \mathcal{O}([\tilde{\epsilon}_X]_{e\alpha}^2)), \quad (2.19)$$

where we define $t_{2\theta_{12}} \equiv \tan(2\theta_{12})$. Here, the $[\tilde{\epsilon}_X]_{e\tau}$ contribution is suppressed by s_{13} and for $[\tilde{\epsilon}_X]_{e\mu}$ is not suppressed. Summarizing, the medium baselines, Daya Bay (DB) [5], RENO [6] and Double Chooz (DC) [4] experiments are more sensitive to $[\tilde{\epsilon}_X]_{e\tau}$ and KamLand [3] is more sensitive to $[\tilde{\epsilon}_X]_{e\mu}$.

In addition to the oscillation terms N_{kl}^{osc} , in Eq. (2.15) there is CP violating term, (N_{kl}^{CP}). In the standard case of oscillation, induced by PMNS mixing matrix the CP violating amplitude (N_{kl}^{CP})^{PMNS} $\rightarrow \text{Im}(J_{kl}^{\alpha\beta})$ where $(J_{kl}^{\alpha\beta}) \equiv U_{\alpha l}^* U_{\beta l} U_{\alpha k} U_{\beta k}^*$ is the Jarlskog invariant [55]. In our setup with $\alpha = \beta = e$, we should have (N_{kl}^{CP})^{PMNS} $\rightarrow 0$, that is, we have *no CP violation for electron neutrino disappearance experiments in PMNS scenario*, but in BSM scenario this term is non-zero and comes from the interference between the standard model with the BSM physics. For the $[\tilde{\epsilon}_X]_{e\mu}([\tilde{\epsilon}_X]_{e\tau})$ parameter the expression for the CP violating term is

$$N_{\text{Sun}}^{\text{CP}} = \left[c_{13}^2 (d_{XL} - p_{XL}) + |[\tilde{\epsilon}_X]_{e\mu}|^2 (d_{XX}p_{XL} - d_{XL}p_{XX}) \right] \text{Im}\{[\tilde{\epsilon}_X]_{e\mu}\} c_{13} s_{2\theta_{12}}, \quad (2.20)$$

$$N_{\text{atm}}^{\text{CP}} = \left[(d_{XL} - p_{XL}) + s_{2\theta_{13}} |[\tilde{\epsilon}_X]_{e\tau}|^2 (d_{XX}p_{XL} - d_{XL}p_{XX}) \right] \text{Im}\{[\tilde{\epsilon}_X]_{e\tau}\} s_{2\theta_{13}}. \quad (2.21)$$

Here, it is explicit that the source of CP violation is the imaginary part of $[\tilde{\epsilon}_X]_{e\beta}$. Another thing that appears is that the CP violation terms are always proportional to the difference $(d_{XL} - p_{XL})$ or the difference $(d_{XX}p_{XL} - p_{XX}d_{XL})$, these two differences are asymmetry between the production and detection process that mimic a T violation in production and detection process. From this we conclude that for CP violating term, the KamLand [3] will be more sensitive to $[\tilde{\epsilon}_X]_{e\mu}$ and the medium baseline to $[\tilde{\epsilon}_X]_{e\beta}$. This is the opposite of what happens for the amplitude of oscillations.

We can compute the equivalent of Jarlskog invariant for the BSM scenario as described in Appendix B. From Eq. (2.20) and Eq. (2.21) we can read that

$$J_{e\mu} = \text{Im}\{[\tilde{\epsilon}_X]_{e\mu}\} c_{13}^3 s_{2\theta_{12}}, \quad (2.22)$$

$$J_{e\tau} = \text{Im}\{[\tilde{\epsilon}_X]_{e\tau}\} s_{2\theta_{13}}. \quad (2.23)$$

As discussed before in the standard neutrino oscillation scenario, when the initial and final neutrino are equal there is no CP violation. Then any evidence of $J_{e\alpha}$, $\alpha = e, \mu \neq 0$ it will signal new physics.

In principle, experiments as Daya Bay (DB) [5], RENO [6] and Double Chooz (DC) [4] are not sensitive to the solar scale terms, Δm_{21}^2 . This is because from eq. (2.17), the effects on the usual neutrino oscillation the Δm_{21}^2 contribution is $(\phi_{21}L)^2$ that is too small. However, for CP violating terms, the amplitude N_{kl}^{CP} is multiplied instead by $\sin(\phi_{kl})$. Due to this the CP violating term can be at the same order of the usual oscillation term from Δm_{31}^2 , this happens when

$$\text{Im}\{[\tilde{\epsilon}_X]_{e\mu}\} s_{2\theta_{12}} \sin(\Delta_{\text{sun}}) \sim s_{2\theta_{13}}^2 \sin^2(\Delta_{\text{atm}}). \quad (2.24)$$

This may cause medium baseline reactors sensitive to CP-violation not only from the atmospheric scales but also from the solar scale. This is shown graphically in Fig. (1), where the medium baseline neutrino reactor experiments, Daya Bay (DB) [5], RENO [6] and Double Chooz (DC) [4] are sensitive to Δm_{21}^2 .

2.2 Flavour conversion in the sun

To arrive at the expressions for the effect of NSI in the solar neutrino data, we return to Eq. (2.4) and (2.5). Unlike reactor neutrinos, the solar neutrino flux arrives at the detectors as an incoherent admixture of mass eigenstates, so the sum in Eq. (2.4) becomes:

$$\frac{R_{\alpha\beta}}{\phi_{\alpha}^{\text{SM}}\sigma_{\beta}^{\text{SM}}} = \sum_{kl} \delta_{kl} \left[\tilde{V}_{\alpha}^{kl}(p_X) \right] \times \left[V_{\beta}^{kl}(d_X) \right]^*. \quad (2.25)$$

Besides, we have to take into account the mixing angle in matter at the production point. Writing explicitly:

$$\begin{aligned} \frac{R_{\alpha\beta}}{\phi_{\alpha}^{\text{SM}}\sigma_{\beta}^{\text{SM}}} &= \sum_k (|\tilde{U}_{\alpha k}|^2 + 2 \text{Re}\{p_{XL}(\epsilon_X \tilde{U})_{\alpha k}^* \tilde{U}_{\alpha k}\}) + |p_{XX}(\epsilon_X \tilde{U})_{\alpha k}|^2 \\ &\times (|U_{\beta k}|^2 + 2 \text{Re}\{d_{XL}(\epsilon_X U)_{\beta k}^* U_{\beta k}\}) + |d_{XX}(\epsilon_X U)_{\beta k}|^2 \end{aligned} \quad (2.26)$$

where \tilde{U} denotes the mixing matrix in the production point inside the Sun. It is clear from Eq. (2.26) that solar neutrinos has no sensitivity to CP violation effects induced by NSI.

As a consistency test, it is straightforward, although cumbersome, to check that Eq. (2.26) reduces to Eq. (2.15) taking the average over the oscillation terms in Eq. (2.15) and making $\tilde{U} \rightarrow U$ in Eq. (2.26). However, it is clearer for solar neutrinos to emphasize the modifications induced by NSI on the initial fluxes and cross-sections.

For instance, for the electron neutrino flux created at the Sun, it is possible to write how such flux is shared between the mass eigenstates:

$$\Phi(\nu_k) = \phi(\nu_e) \left(P_{ek}^{\text{SM}} + 2 \text{Re} \left\{ p_{\text{XL}}(\epsilon_X \tilde{U})_{\alpha k}^* \tilde{U}_{\alpha k} \right\} + |p_{\text{XX}}(\epsilon_X \tilde{U})_{\alpha k}|^2 \right) \quad (2.27)$$

and, similarly, the effective cross-section of detecting a β -flavour neutrino on Earth from a mass eigenstate k can be written as:

$$\sigma_\beta = \sigma_\beta^{\text{SM}} \left(P_{k\beta}^{\text{SM}} + 2 \text{Re} \left\{ d_{\text{XL}}(\epsilon_X U)_{\beta k}^* U_{\beta k} \right\} + |d_{\text{XX}}(\epsilon_X U)_{\beta k}|^2 \right) \quad (2.28)$$

With these expressions, we can implement the NSI effects as corrections on production probabilities of mass eigenstates in the Sun and corresponding probabilities of detecting a mass eigenstate at the detectors. However, it is essential to note that these are not actual probabilities, not adding to 1 when all states are considered.

Using the same ansatz given by Eqs. (2.12) to Eq. (2.12) (but for neutrinos), we present in the following the corrections on such probabilities.

For solar production of mass eigenstates and $\tilde{\epsilon}_{e\mu}$, we have:

$$\begin{aligned} P_{e1} &\rightarrow P_{e1}^{\text{SM}} - 2 \text{Re} \{ [\tilde{\epsilon}_X]_{e\mu} \} p_{\text{XL}} \tilde{s}_{12} \tilde{c}_{12} c_{13} + |[\tilde{\epsilon}_X]_{e\mu}|^2 p_{\text{XX}} \tilde{s}_{12}^2 \\ P_{e2} &\rightarrow P_{e2}^{\text{SM}} + 2 \text{Re} \{ [\tilde{\epsilon}_X]_{e\mu} \} p_{\text{XL}} \tilde{s}_{12} \tilde{c}_{12} c_{13} + |[\tilde{\epsilon}_X]_{e\mu}|^2 p_{\text{XX}} \tilde{c}_{12}^2 \\ P_{e3} &= P_{e3}^{\text{SM}} \end{aligned} \quad (2.29)$$

For $\tilde{\epsilon}_{e\tau}$, we have:

$$\begin{aligned} P_{e1} &\rightarrow P_{e1}^{\text{SM}} - 2 \text{Re} \{ [\tilde{\epsilon}_X]_{e\mu} \} p_{\text{XL}} \tilde{c}_{12}^2 s_{13} c_{13} + |[\tilde{\epsilon}_X]_{e\mu}|^2 p_{\text{XX}} \tilde{c}_{12}^2 s_{13}^2 \\ P_{e2} &\rightarrow P_{e2}^{\text{SM}} - 2 \text{Re} \{ [\tilde{\epsilon}_X]_{e\mu} \} p_{\text{XL}} \tilde{s}_{12}^2 s_{13} c_{13} + |[\tilde{\epsilon}_X]_{e\mu}|^2 p_{\text{XX}} \tilde{s}_{12}^2 s_{13}^2 \\ P_{e3} &= P_{e3}^{\text{SM}} + 2 \text{Re} \{ [\tilde{\epsilon}_X]_{e\mu} \} p_{\text{XL}} c_{13} + |[\tilde{\epsilon}_X]_{e\mu}|^2 p_{\text{XX}} \tilde{c}_{13}^2 \end{aligned} \quad (2.30)$$

and for the detection on Earth we obtain similar expressions, with $d_{XL} \rightarrow p_{XL}$ and $\tilde{U} \rightarrow U$.

We can note that for $\tilde{\epsilon}_{e\tau}$ the corrections on the probabilities involving the two first families, which are the most relevant for solar neutrinos, are suppressed by the small value of θ_{13} . Indeed, we explicitly checked that the constraints on $[\tilde{\epsilon}_X]_{e\tau}$ from solar neutrino data are much weaker than those coming from reactor neutrino experiments.

As stated above, we assume that the probabilities in solar neutrino flux can be treated classically since the flux is an incoherent sum of mass eigenstates. However, if the neutrinos arrive at the detector during the night, the coherence between mass eigenstates is reestablished, and flavour oscillation can be probed. We developed expressions to include NSI on neutrino regeneration on Earth and explicitly checked that its effect on the constraints is marginal.

2.2.1 Solar neutrino production and detection factors

For the solar neutrinos, we assume mainly Gamow-Teller production. As in the reactor case, we use the Lagrangian of Eqs. (1.1), and we always consider each type of non-standard interaction per time.

	scalar	tensor		scalar	tensor
p_{XL}	0	$+\frac{g_T}{g_A} \frac{m_e}{E_e}$	p_{XX}	$\frac{g_S^2}{3g_A^2}$	$\frac{g_T^2}{g_A^2}$
d_{XL}	$-\frac{g_S g_V}{g_V^2 + 3g_A^2} \frac{m_e}{E_e}$	$\frac{3g_A g_T}{g_V^2 + 3g_A^2} \frac{m_e}{E_e}$	d_{XX}	$\frac{g_S^2}{g_V^2 + 3g_A^2}$	$\frac{3g_T^2}{g_V^2 + 3g_A^2}$

Table 2. The same as Table 1 but now for production and detection factors for solar neutrinos.

In general, the neutrino production in the solar core comes from several chain reactions including proton-proton collisions and beta decays. In this work, we restrict ourselves to beta decays (in the solar case, the β^+). As a result, any other production mechanism will be the same as in the standard model. The detection, will be considered as inverse beta decays, β^- :

$$\begin{aligned} \beta^+ : {}^A_Z N_i &\rightarrow {}^A_{Z-1} N_f + e^+ + \nu_e, & (\text{production}) \\ \text{inv. } \beta^- : {}^A_Z N_i + \nu_e &\rightarrow e^- + {}^A_{Z+1} N_f, & (\text{detection}) \end{aligned} \quad (2.31)$$

The p_{XY} and d_{XL} , Eq. (2.6), for the sun are presented in table 2. We follow the same notation as in table 1.

3 Analysis details

3.1 Medium baseline reactors

Here we explore the reactors medium baseline experiments: Daya Bay [5], RENO [6] and Double Chooz [4], those are considered Medium Baseline Reactors (MBR) and are sensitive to the Δm_{31}^2 . For that case, we use the GlobesFit code [56] modified to include non-standard interactions. For further details on the experimental setup see [56]. For the MBR case, we adopt the following χ^2 distribution:

$$\chi_{\text{MBR}}^2 = \sum_{\text{exp}=\{\text{DB,DC,RENO}\}} (\chi_{\text{exp}}^{\text{shape}})^2 + (\chi_{\text{exp}}^{\text{rate}})^2 + \frac{(1-\alpha)^2}{\sigma_a^2}, \quad (3.1)$$

where,

$$(\chi^2)_{\text{DB}}^{\text{shape}} = \sum_{k=\{\text{EH2,EH3}\}} \sum_{i,j}^{N_{\text{DB}}} (d_i^k - n_i^k)(V_{\text{DB}}^{-1})_{ij}(d_j^k - n_j^k), \quad (3.2)$$

here, d_i^k is the released data on the energy bin i (over $N_{\text{DB}} = 52$ energy bins) for the ratio between the number events in the experimental hall k (EHk) with EH1, n_i^k is the

corresponding simulated value. Here V_{db} is the covariance matrix for the Daya Bay shape analysis. And

$$(\chi^2)_{\text{DB}}^{\text{rate}} = \sum_{i,j}^{N_{\text{DB}}} (d_{0,i}^k - (1 - \alpha)n_{0,i}^k)(W_{\text{DB}}^{-1})_{ij}(d_{0,j}^k - (1 - \alpha)n_{0,j}^k), \quad (3.3)$$

where the variable have similar meanings as in the shape analysis case, with the difference that $d_{0,i}(n_{0,i})$ (i runs over $N_{\text{DB}} = 8$ bins for different running periods) is the ratio between the total number of events at AD1, AD2, AD8 and AD3 divided by the standard oscillation prediction case. The parameters α controls the normalization error, $\sigma_a = 0.025$, that we assume to be fuel independent. For Double Chooz (DC) ($N_{\text{DC}} = 26$ data points in the shape analysis and 4 data points in the rate) and RENO ($N_{\text{RENO}} = 25$ data points in the shape analysis and 8 data points in the rate) we consider near and far detectors ratio. The χ^2 is the same as in Eqs. (3.2) and (3.3) but d_i^k is the far/near ratios and $d_{0,i}^k$ are the ratios in the near detector with the standard model prediction.

3.2 KamLand experiment

In this section, we describe the setup we used to simulate KamLand experiment [3]. The KamLand experiment consists of 1 kton of highly purified liquid scintillator detector in Japan that collects signals of inverse beta decay of neutrinos coming from different reactors in Japan. As the average distance from the reactors and the KamLand detector is of the order of 180 km, and the neutrino energies are around 3 MeV, the experiment is sensitive to the solar neutrino mass squared difference Δm_{21}^2 .

The KamLand detector measures the event rates for the anti-neutrino signal from 2002 to 2007. The total exposure of the experiment was 2.44×10^{32} proton-yr. We consider the KamLand number of neutrino events in a bin as given by:

$$n_i \propto \epsilon_i \int_{E_i^{\text{min}}}^{E_i^{\text{max}}} dE_e \int_{E_{\text{th}}}^{\infty} dE_\nu \left(\sum_j W_j \left(\frac{R_{\bar{\nu}_e \bar{\nu}_e}}{\phi_e^{\text{SM}} \sigma_e^{\text{SM}}} \right)_{(E_\nu, L_j)} \right) \frac{d\Phi(E_\nu)}{dE_\nu} \frac{d\sigma(E_\nu)}{dE_e} R(E_\nu, E_R), \quad (3.4)$$

where the ϵ_i is the efficiency of the bin, E_ν is the neutrino energy, E_{th} is the threshold energy for the neutrino interaction, E_e is the positron energy, $R(E_\nu, E_R)$ is the energy resolution function, W_j is the power of the j -th reactor, $\left(\frac{R_{\bar{\nu}_e \bar{\nu}_e}}{\phi_e^{\text{SM}} \sigma_e^{\text{SM}}} \right)_{(E_\nu, L_j)}$ will be given by the oscillation rate Eq. (2.4), $\frac{d\sigma(E_\nu)}{dE_e}$ is the detection differential cross-section and the anti-neutrino flux at the detector is given by

$$\frac{d\Phi(E_\nu)}{dE_\nu} = \frac{\sum_j F_j \frac{d\phi_\nu^{(j)}(E_\nu)}{dE_\nu}}{4\pi \sum_i W_i L_i^2}, \quad (3.5)$$

where F_j are the fraction of the reactor fuel given by KamLand collaboration (0.567 : 0.078 : 0.298 : 0.057) for (^{235}U : ^{238}U : ^{239}Pu : ^{241}Pu). The neutrino flux comes from [57] and the baselines L_i and power W_i for each reactor comes from [58]. The efficiencies are

given by ϵ_i and extracted from [3]. The anti-neutrino cross-section comes from [59] and the neutrino reconstruction function was used [60] using a $6.4\% \sqrt{E_\nu(\text{MeV})}$ error given by [3].

For the statistical analyse of KamLand (KL), we calculate the following χ^2 :

$$\chi_{\text{KL}}^2 = \sum_i \frac{\left(d_i - n_i(a_1, a_2) - b_i(a_3, a_4)\right)^2}{d_i} + \sum_i \frac{a_i^2}{\sigma_i^2} \quad (3.6)$$

where d_i is the data extracted by summing the number of events of the three KamLand phases of Ref. [3], b_i is the background also extracted from Ref. [3], σ_i are systematic errors, we used $\sigma_1 = 0.05$ (signal normalization error), $\sigma_2 = 0.02$ (signal energy error), $\sigma_3 = 0.08$ (background normalization error) and $\sigma_4 = 0.02$ (background energy error). Also, the number of events given the calibration and normalization errors will be the same as in the Ref. [61]:

$$n_i(a, b) = (1 + b)(1 + a) \left[(n_{i+1} - n_i)(\delta(b) - i) + n_i \right], \quad (3.7)$$

here, $\delta(b) = b(i + t_0 + 0.5) + i$ where $t_0 = N_{\text{bins}} E_{\text{min}} / (E_{\text{max}} - E_{\text{min}})$. For each χ_{KL}^2 we minimize over the nuisance parameters a_i .

3.3 Solar experiments

For the solar neutrino data, we perform a statistical analysis following the same procedure presented in [62, 63]. The solar neutrino data used are:

- the full spectral data from Super-Kamiokande phases I, III and IV [10–12];
- the combined analysis of all three SNO phases [13];
- Borexino results [14];
- combined Gallex+GNO [15] and SAGE [16] data;
- Homestake results [17].

3.4 Global picture

For our analysis of the global electron disappearance we can adopt the uncorrelated test statistics summing the χ^2 functions, Eqs. (3.1),(3.6) and χ_{Sun}^2 , for MBR, Kamland and solar data:

$$\chi_{\text{global}}^2 = \chi_{\text{MBR}}^2 + \chi_{\text{KL}}^2 + \chi_{\text{Sun}}^2. \quad (3.8)$$

When the $[\tilde{\epsilon}_X]_{e\tau}$ parameter is present, we assume the MBR to be dependent on Δm_{31}^2 and θ_{13} . On the other hand if $[\tilde{\epsilon}_X]_{e\mu}$ is considered we also include the Δm_{21}^2 fixing $\theta_{12} = 33.4^\circ$, this was made because the CP-violation term of the solar scale is not negligible in the MBR scale. For KamLand, the θ_{13} , Δm_{21}^2 and θ_{12} are considered for both $[\tilde{\epsilon}_X]_{e\tau}$ and $[\tilde{\epsilon}_X]_{e\mu}$. In the solar scenario, we neglect $[\tilde{\epsilon}_X]_{e\tau}$ because it is always suppressed for a small θ_{13} . For the $[\tilde{\epsilon}_X]_{e\mu}$ inclusion in the sun, the χ^2 will also depend on θ_{13} , Δm_{21}^2 and θ_{12} .

4 Results

In this analysis, we consider the solar, KamLand, and MBR experiments. We use a total of 280 data points, 149 from solar experiments, 17 from KamLand, and 114 for the MBR (shape+rate analysis). As expected, the Standard Oscillation produces a fit that is in good agreement with the data giving the minimum of the global χ^2 : $\{\chi_{\min}^2\} = 242.6$ as shown in Table (3). In the standard oscillation 4 parameters were considered: θ_{13} , θ_{12} , Δm_{31}^2 and Δm_{21}^2 under the normal ordering hypothesis. Individually, each of those experiments also is in agreement with the data ($\min\{\chi_{\text{KL}}^2\} = 15.0$, $\min\{\chi_{\text{Sun}}^2\} = 134.0$ and $\min\{\chi_{\text{KL}+\text{Sun}}^2\} = 155.1$), the solar and KamLand are sensitive to θ_{12} , Δm_{21}^2 and can alone put a weak maximum size for θ_{13} . The MBR experiments are either in agreement with data, leading to $\min\{\chi_{\text{MBR}}^2\} = 87.0$ and are sensitive to θ_{13} and Δm_{31}^2 .

	S.O.	$[\tilde{\epsilon}_S]_{e\tau}$	$[\tilde{\epsilon}_T]_{e\tau}$	$[\tilde{\epsilon}_S]_{e\mu}$	$[\tilde{\epsilon}_T]_{e\mu}$	n_{data}
$(\{\chi_{\text{Sun}}^2\})_{\min}$	134.0	134.0	134.0	133.9	132.0	149
$(\{\chi_{\text{KL}}^2\})_{\min}$	15.0	14.9	14.5	15.0	14.6	17
$(\{\chi_{\text{MBR}}^2\})_{\min}$	87.0	84.1	85.1	83.9	82.5	87
$(\{\chi_{\text{GLOBAL}}^2\})_{\min}$	242.7	240.3	241.3	242.3	239.9	280
$\Delta\bar{\chi}_{\text{PG}}^2$ (p-value)	15.7%	29.0%	26.0%	38.3%	10.8%	—

Table 3. Summary of the analysis, here $(\{\chi_X^2\})_{\min}$ is the minimum χ^2 for experiment X=medium baseline reactor experiments, KamLand and solar experiments and $\Delta\bar{\chi}_{\text{PG}}^2 \equiv (\{\chi_{\text{GLOBAL}}^2\})_{\min} - \sum_i (\{\chi_X^2\})_{\min}$. The number of data points, n_{data} , are shown in the last column.

When considering NSI, we noticed that KamLand and Solar experiments are more sensitive to $[\tilde{\epsilon}_X]_{e\mu}$ than in MBR. On the other hand, the MBR sensitivity to $[\tilde{\epsilon}_X]_{e\tau}$ is much more robust than in the KamLand and solar experiment, turning their contribution negligible to the global analysis. Those sensitivity associations can be graphically seen in Fig. 1. Finally, in Tab. 3, we summarize the relevant statistical results of this work that will be presented in detail in the next sections.

4.1 The $[\tilde{\epsilon}_X]_{e\tau}$ analysis

For the $[\tilde{\epsilon}_X]_{e\tau}$ parameter, the leading contributions come from MBR. In KamLand and solar experiments, the $[\tilde{\epsilon}_X]_{e\tau}$ NSI parameters are always suppressed by a small θ_{13} leading to little changes in the analysis. Hence, we will consider only MBR for the $[\tilde{\epsilon}_X]_{e\tau}$ analysis. The resulting medium baseline reactors χ^2 functions, Eq. (3.1), is shown in Fig. 2 for scalar and tensor interactions.

For scalar $[\tilde{\epsilon}_S]_{e\tau}$ interactions, the Standard Oscillation is disfavored by 1.73σ in comparison with the NSI scenario. In Fig. 2, we can see that a correlation between Δm_{31}^2 and the CP violation term (imaginary part of $[\tilde{\epsilon}_S]_{e\tau}$) drives to an improvement in the fit leading to a large $\Delta m_{31}^2 = 2.78 \times 10^{-3} \text{ eV}^2$ and non-zero $\text{Im}[\tilde{\epsilon}_S]_{e\tau} = +0.62$. The analysis also leads to a 3σ allowed region of $\sin^2\theta_{13} \approx 0.05$. The values of the real and imaginary parts of $[\tilde{\epsilon}_S]_{e\tau}$ are

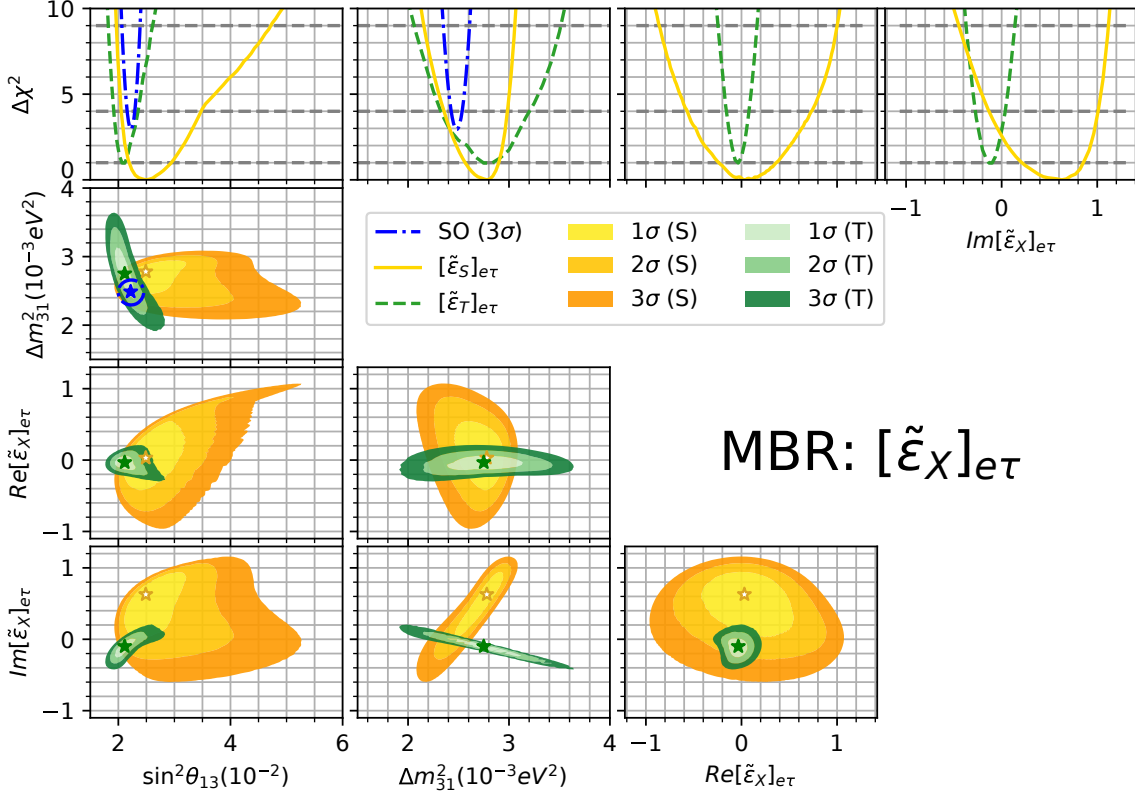


Figure 2. Upper panel: The 1D projection of the $\Delta\chi^2 \equiv \chi^2 - \chi^2_{\text{minimum}}$ of medium baseline reactors (MBR) in the presence of $[\tilde{\epsilon}_X]_{e\tau}$ for the different parameters. Lower panels the contour levels for oscillations parameters and the BSM couplings at 1σ , 2σ and 3σ . In green (yellow) is the NSI tensor (scalar) case and in dash-dotted black is standard oscillation case.

$$\text{Re}[\tilde{\epsilon}_S]_{e\tau} = +0.03_{-0.21}^{+0.40}, \quad \text{Im}[\tilde{\epsilon}_S]_{e\tau} = +0.62_{-0.41}^{+0.23}. \quad (4.1)$$

In the tensor interaction case, the Standard Model is disfavored by a 1.41σ statistical significance, see Fig. 2. As in the scalar case, the Δm^2_{31} is correlated to the imaginary part of the NSI also leading to a larger value of $\Delta m^2_{31} = 2.75 \times 10^{-3} \text{ eV}^2$ but now the imaginary part is $\text{Im}[\tilde{\epsilon}_T]_{e\tau} = +0.12$. At 3σ in the tensor case the Δm^2_{31} can reach values of $3.6 \times 10^{-3} \text{ eV}^2$ and $\sin^2 \theta_{13} = 0.027$ upper limit at 3σ . The values of the real and imaginary parts of the NSI parameter are:

$$\text{Re}[\tilde{\epsilon}_T]_{e\tau} = -0.03_{-0.06}^{+0.06}, \quad \text{Im}[\tilde{\epsilon}_T]_{e\tau} = -0.12_{-0.10}^{+0.08}. \quad (4.2)$$

4.2 The $[\tilde{\epsilon}_X]_{e\mu}$ analysis

We will divide this section for the $[\tilde{\epsilon}_X]_{e\mu}$ analysis, first presenting the results for MBR and finishing with the global analysis where we combine the MBR with solar and Kamland experiments.

In the MBR analysis, we found an improvement in the statistics for both tensor and scalar interactions, compared to the standard model analysis ($\min\{\chi^2_{\text{SM}}\} = 87.0$). In

the tensor interactions, we found $\min\{\chi^2\} = 82.5$ and in the scalar case, $\min\{\chi^2\} = 83.9$. In both cases, tensor and scalar interaction, the improvement in the analysis comes mainly from a non-zero CP violation effect of the Δm_{21}^2 , Eq. (2.24), that affects the MBR experiments. As this is an effect that comes from the solar sector of the oscillation probability, the θ_{13} and Δm_{31}^2 does not change in the same size as in the $[\tilde{\epsilon}_X]_{e\tau}$ analysis, see Fig. 3. In Fig. 3 we show the χ^2 contours for the analysis of MBR reactors, respectively, for scalar (yellow) and tensor (green) interactions. In the case of scalar interactions, the Standard Model is disfavored by 1.8σ , with the best fit on $\text{Im}[\tilde{\epsilon}_S]_{e\mu} = -0.90$. In contrast with the $e\tau$ NSI, the $e\mu$ does not include big changes and correlations in the Standard Oscillation parameters. As mentioned, the imaginary effect of the $e\mu$ parameter in MBR experiments comes from the solar scale CP violation term. For the case of the tensor interactions, Fig. 3, the significance reaches 2.1σ with $\text{Im}[\tilde{\epsilon}_T]_{e\mu} = 0.44$ and accommodating a larger value of $\Delta m_{31}^2 = 2.68 \times 10^{-3} \text{ eV}^2$.

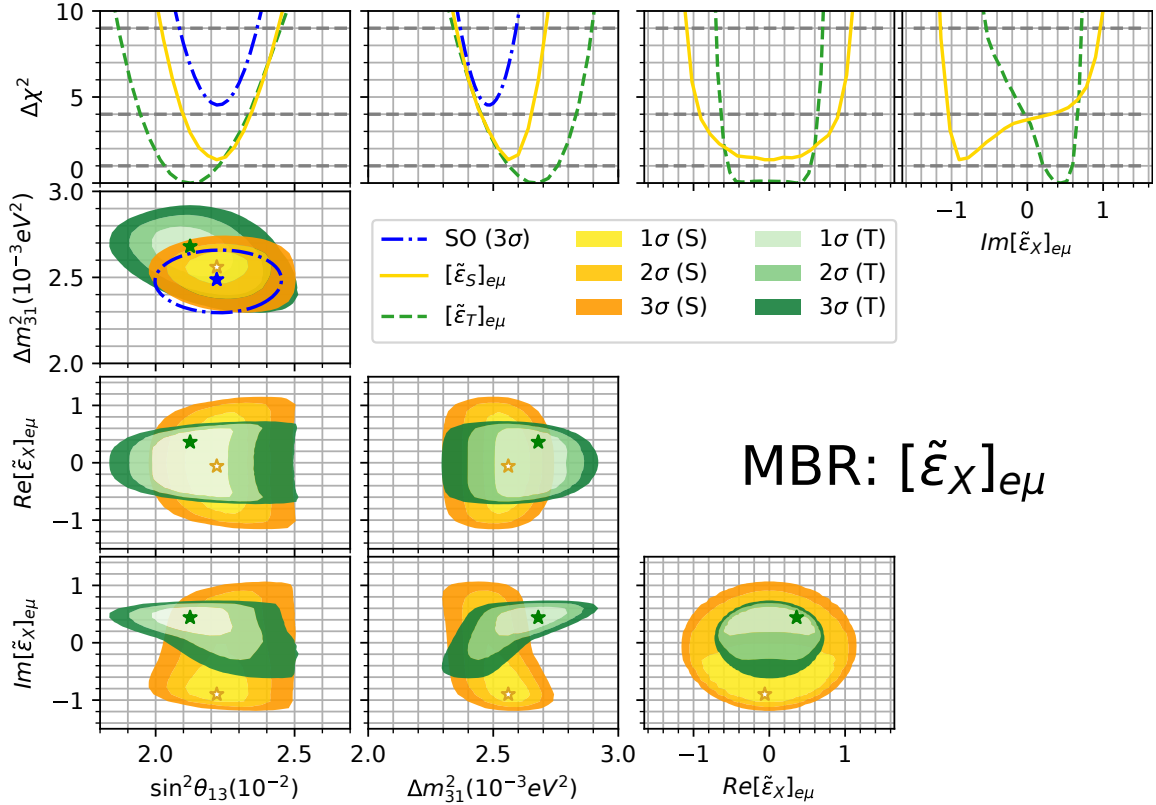


Figure 3. The same as in fig. 2 but for $[\tilde{\epsilon}_X]_{e\mu}$ interactions.

In general, the $e\mu$ interactions will be sensitive also in KamLand and solar experiments where the NSI receives its strongest bounds (mainly from solar data). The combined analysis of scalar and tensor interactions are presented in Fig. 4. In the presence of scalar $e\mu$ interactions, there is no change in the statistical significance compared to the Standard Model. Also, the standard model parameters Δm_{21}^2 and θ_{12} have only small changes except for the θ_{13} as can be seen in Fig. 4. The main source of limits on the $[\tilde{\epsilon}_S]_{e\mu}$ comes from

solar experiments. For the global analysis of $[\tilde{\epsilon}_S]_{e\mu}$, the $\Delta\chi^2$ curves can be seen on Fig. 4 where $\Delta\chi^2_{\min} = 242.28$. From the global analysis of the $[\tilde{\epsilon}_S]_{e\mu}$ interactions, the limits on the NSI parameters are:

$$\text{Re}[\tilde{\epsilon}_S]_{e\mu} = 0.00 \pm 0.25, \quad \text{Im}[\tilde{\epsilon}_S]_{e\mu} = -0.16^{+0.31}_{-0.09}. \quad (4.3)$$

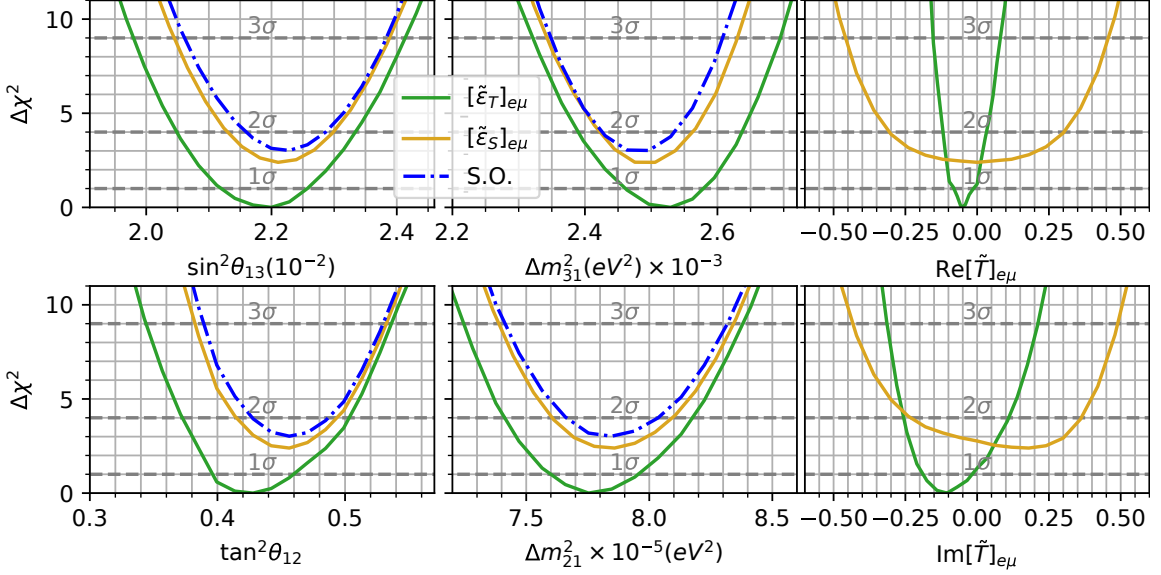


Figure 4. Here we show the global $\Delta\chi^2$ curves in the case of active $[\tilde{\epsilon}_X]_{e\mu}$. In we show the NSI scenario and in dashed-dotted blue, the standard oscillation scenario (S.O.).

In the case of tensor interactions for the KamLand+Solar analysis, there is an improvement of 1.3σ in the statistics compared with the Standard Model (more information for the KamLand +Solar analysis are presented in the Appendix C). In the global analysis case, there is an improvement of around 1.7σ compared to the standard model scenario. The global analysis results are presented in Fig. 4. The values of the NSI parameters for the $[\tilde{\epsilon}_T]_{e\mu}$ are:

$$\text{Re}[\tilde{\epsilon}_T]_{e\mu} = -0.05^{+0.04}_{-0.03}, \quad \text{Im}[\tilde{\epsilon}_T]_{e\mu} = -0.13^{+0.09}_{-0.07}. \quad (4.4)$$

Summarizing the analysis for all interactions, the boxplot for the distributions of the parameters is shown in Fig. 5. In green, we show the tensor interactions, in yellow the scalar interactions, and the standard model. From Fig. 5 one can see that the main changes appear in the θ_{13} and Δm^2_{31} parameters when $[\tilde{\epsilon}_X]_{e\tau}$ interactions are present. Also large CP violation effects were found for $[\tilde{\epsilon}_S]_{e\tau}$ and $[\tilde{\epsilon}_T]_{e\mu}$. We discuss in more detail the CP violation effects in the next section.

In the next section, we present our results using the Eq. (3.8) to estimate the standard and non-standard parameter values. Moreover, in order to check the parameter consistency over different data sets, it can also be interesting to calculate the parameters goodness of fit [64] for the NSI values, by using the:

$$\Delta\bar{\chi}^2 = \Delta\chi^2_{\text{MBR}} + \Delta\chi^2_{\text{KL}} + \Delta\chi^2_{\text{Sun}}, \quad (4.5)$$

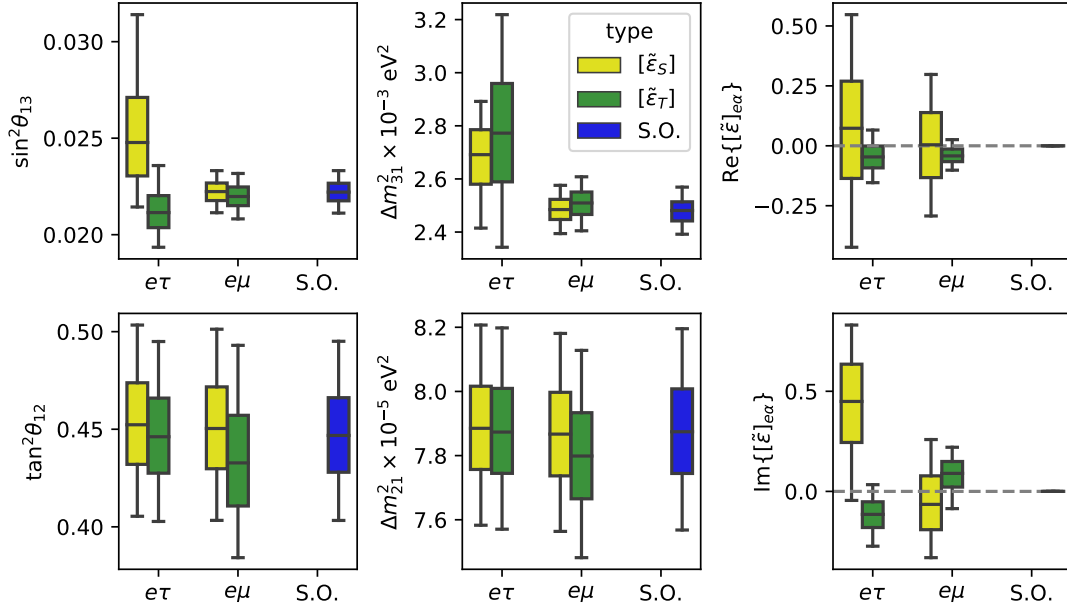


Figure 5. The boxplot for the parameters distributions. We show the median, the first and third quartile boxes and the 5% and 95% percentiles for the whiskers ($\approx 90\%$ C.L.).

where the $\min(\Delta\bar{\chi}^2)$ is distributed as a χ^2 statistics with $P_c = \sum_r P_r - P = 5 + 5 + 5 - 6 = 9$ d.o.f. for $[\tilde{\xi}_X]_{e\mu}$ and $P_c = \sum_r P_r - P = 4 + 5 + 3 - 6 = 6$ d.o.f. for $[\tilde{\xi}_X]_{e\tau}$.

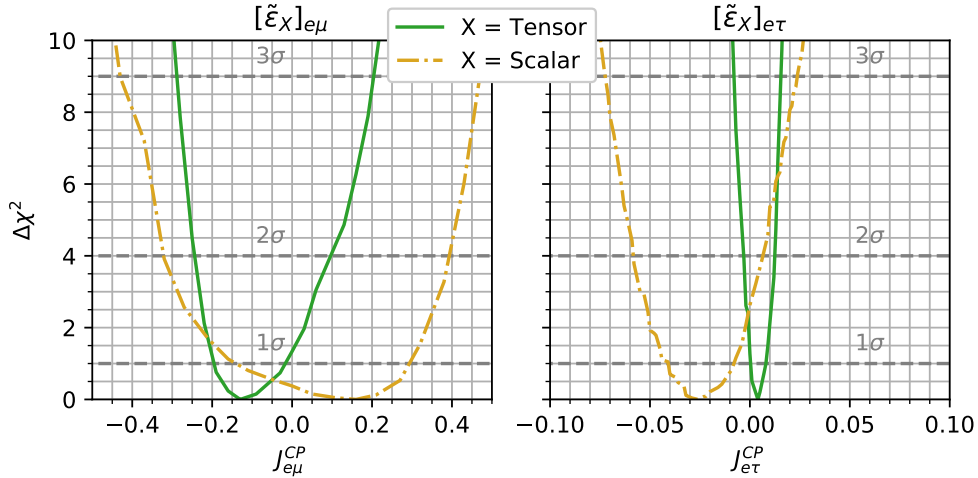


Figure 6. In this figure we show the CP-violation parameters of Eqs. (2.23) and (2.22). In the left (right) panel we show the $e\tau$ ($e\mu$) parameters. In green is for Tensor interactions and in yellow for scalar interactions.

4.3 CP violation

In this section, we quantify the effects of the CP violation terms, as presented in Eqs. (2.22) and (2.23). The results can be seen in Fig. 6; in the left panel, we show the $\Delta\chi^2$ curve for the

$e\mu$ interactions and in the right panel for the $e\tau$ interactions. In plain green are shown the tensor interactions in which the strength of CP is more constrained than the dash-dotted yellow. There are two scenarios, $[\tilde{\epsilon}_T]_{e\mu}$ and $[\tilde{\epsilon}_S]_{e\tau}$, where a preference for non-zero CP violation in more than 1σ appears. For the tensor, $[\tilde{\epsilon}_T]_{e\tau}$ interactions, the constraint is the most restrictive. On the other hand, for the $[\tilde{\epsilon}_S]_{e\mu}$, the bounds are more relaxed.

For the $[\tilde{\epsilon}_T]_{e\mu}$ and $[\tilde{\epsilon}_S]_{e\tau}$ cases, we draw the event ratios in the best-fit point for Daya Bay with CP violation, the dashed green and dashed-dotted yellow. We further draw the lines when we fixed by hand the CP violation term to zero, the dotted lines.

5 Conclusions

We studied the effects on non-standard neutrino interaction in the production and detection of neutrinos and compare with the medium baseline reactors experiments, Daya Bay, RENO, Double Chooz, KamLand and solar experiments.

Usually the non-standard neutrino interaction in the production and detection of neutrinos are assumed constants independent of energy. We follow the approach of [45, 47] to compute the changes in neutrino production and detection assuming scalar and tensorial interactions. This approach have interesting characteristics as the amplitudes of the oscillation are *now energy dependent*, due the interference of scalar/tensorial amplitude with standard model amplitudes. We decide to test this scenario for experiments with (anti)-electron neutrino in initial and in the final state as shown in eq.(2.4). This scenario test the flavor structure of electron disappearance experiments due the NSI parameters $[\tilde{\epsilon}_X]_{e\mu}$ and $[\tilde{\epsilon}_X]_{e\tau}$. A side effect of this approach is that, we will *CP violation effects*, due the imaginary part of non-standard couplings, even when the initial and final neutrinos are the same.

The summary of our results are shown in table (3) and in figure (5). The highlights of our scenario a slight preference ($\sim 1\sigma$) for non-zero CP violation effects as the best-fit in all scenarios that we studied. For only reactor neutrino experiments, for the parameter $[\tilde{\epsilon}_X]_{e\tau}$ the results are in figure (2) that shown the increase in the allowed region of mixing angles and mass differences, mostly for $\sin^2 \theta_{13}$ and Δm_{31}^2 . The inclusion of solar and KamLand experiments did not change much the results of reactor experiments. For the coupling $[\tilde{\epsilon}_X]_{e\mu}$, we have similar results, but here the KamLand and the solar neutrino experiments give good bounds on $[\tilde{\epsilon}_X]_{e\mu}$.

We test the parameter goodness-of-fit of all the parameters, see Eq. (4.5). We find a small improvement compared to the standard model as can be seen in Table 3, the p-value for the standard model is 15.7%, for the non-standard scenario runs from 26% for $[\tilde{\epsilon}_T]_{e\tau}$ to 38.3% in the $[\tilde{\epsilon}_S]_{e\mu}$ scenario. So, in all cases we have an agreement for the parameters in different experiments.

In all cases, we found strong limits on NSI, Eqs. (4.1), (4.2), (4.3) and (4.4), the more restrictive bounds as far as we know. Furthermore, a possibility of different values of Δm_{31}^2 , the summary of the limits on the NSI and on the Standard Oscillation parameters can be seen in fig. 5.

Acknowledgments

P.C.H and O.L.G.P. were thankful for the support of FAPESP funding Grant 2014/19164-6. O.L.G.P were thankful for the support of FAEPEX funding grant 2391/2017 and 2541/2019, CNPq grant 306565/2019-6. M.E.C. is thankful for 140564/2018-7 funding from CNPQ and 88887.477371/2020-00 funding from CAPES. The authors are thankful to Zahra Tabrizi, Marcelo Guzzo and Yago Porto for useful discussions about the topic. This study was financed in part by the Coordenação de Aperfeiçoamento de Pessoal de Nível Superior - Brasil (CAPES) - Finance Code 001.

References

- [1] SUPER-KAMIOKANDE collaboration, Y. Fukuda et al., *Evidence for oscillation of atmospheric neutrinos*, *Phys. Rev. Lett.* **81** (1998) 1562 [[hep-ex/9807003](#)].
- [2] SNO collaboration, Q. R. Ahmad et al., *Direct evidence for neutrino flavor transformation from neutral current interactions in the Sudbury Neutrino Observatory*, *Phys. Rev. Lett.* **89** (2002) 011301 [[nucl-ex/0204008](#)].
- [3] KAMLAND collaboration, A. Gando et al., *Reactor On-Off Antineutrino Measurement with KamLAND*, *Phys. Rev. D* **88** (2013) 033001 [[1303.4667](#)].
- [4] DOUBLE CHOOZ collaboration, H. de Kerret et al., *Double Chooz θ_{13} measurement via total neutron capture detection*, *Nature Phys.* **16** (2020) 558 [[1901.09445](#)].
- [5] DAYA BAY collaboration, D. Adey et al., *Measurement of the Electron Antineutrino Oscillation with 1958 Days of Operation at Daya Bay*, *Phys. Rev. Lett.* **121** (2018) 241805 [[1809.02261](#)].
- [6] RENO collaboration, G. Bak et al., *Measurement of Reactor Antineutrino Oscillation Amplitude and Frequency at RENO*, *Phys. Rev. Lett.* **121** (2018) 201801 [[1806.00248](#)].
- [7] T2K collaboration, K. Abe et al., *Improved constraints on neutrino mixing from the T2K experiment with 3.13×10^{21} protons on target*, *Phys. Rev. D* **103** (2021) 112008 [[2101.03779](#)].
- [8] NOVA collaboration, M. A. Acero et al., *First Measurement of Neutrino Oscillation Parameters using Neutrinos and Antineutrinos by NOvA*, *Phys. Rev. Lett.* **123** (2019) 151803 [[1906.04907](#)].
- [9] MINOS+ collaboration, P. Adamson et al., *Precision Constraints for Three-Flavor Neutrino Oscillations from the Full MINOS+ and MINOS Dataset*, *Phys. Rev. Lett.* **125** (2020) 131802 [[2006.15208](#)].
- [10] SUPER-KAMIOKANDE collaboration, J. Hosaka et al., *Solar neutrino measurements in super-Kamiokande-I*, *Phys. Rev.* **D73** (2006) 112001 [[hep-ex/0508053](#)].
- [11] SUPER-KAMIOKANDE collaboration, S. Fukuda et al., *Determination of solar neutrino oscillation parameters using 1496 days of Super-Kamiokande I data*, *Phys. Lett.* **B539** (2002) 179 [[hep-ex/0205075](#)].
- [12] SUPER-KAMIOKANDE collaboration, K. Abe et al., *Solar Neutrino Measurements in Super-Kamiokande-IV*, *Phys. Rev.* **D94** (2016) 052010 [[1606.07538](#)].

- [13] SNO collaboration, B. Aharmim et al., *Combined Analysis of all Three Phases of Solar Neutrino Data from the Sudbury Neutrino Observatory*, *Phys. Rev.* **C88** (2013) 025501 [[1109.0763](#)].
- [14] BOREXINO collaboration, M. Agostini et al., *Comprehensive measurement of pp-chain solar neutrinos*, *Nature* **562** (2018) 505.
- [15] F. Kaether, W. Hampel, G. Heusser, J. Kiko and T. Kirsten, *Reanalysis of the GALLEX solar neutrino flux and source experiments*, *Phys. Lett.* **B685** (2010) 47 [[1001.2731](#)].
- [16] SAGE collaboration, J. N. Abdurashitov et al., *Measurement of the solar neutrino capture rate with gallium metal. III: Results for the 2002–2007 data-taking period*, *Phys. Rev.* **C80** (2009) 015807 [[0901.2200](#)].
- [17] B. T. Cleveland, T. Daily, R. Davis, Jr., J. R. Distel, K. Lande, C. K. Lee et al., *Measurement of the solar electron neutrino flux with the Homestake chlorine detector*, *Astrophys. J.* **496** (1998) 505.
- [18] I. Esteban, M. C. Gonzalez-Garcia, M. Maltoni, T. Schwetz and A. Zhou, *The fate of hints: updated global analysis of three-flavor neutrino oscillations*, *JHEP* **09** (2020) 178 [[2007.14792](#)].
- [19] HYPER-KAMIOKANDE PROTO- collaboration, K. Abe et al., *Physics potential of a long-baseline neutrino oscillation experiment using a J-PARC neutrino beam and Hyper-Kamiokande*, *PTEP* **2015** (2015) 053C02 [[1502.05199](#)].
- [20] DUNE collaboration, B. Abi et al., *The DUNE Far Detector Interim Design Report Volume 1: Physics, Technology and Strategies*, [1807.10334](#).
- [21] JUNO collaboration, F. An et al., *Neutrino Physics with JUNO*, *J. Phys. G* **43** (2016) 030401 [[1507.05613](#)].
- [22] K. Chakraborty, D. Dutta, S. Goswami and D. Pramanik, *Invisible neutrino decay : First vs second oscillation maximum*, *JHEP* **05** (2021) 091 [[2012.04958](#)].
- [23] Y. P. Porto-Silva, S. Prakash, O. L. G. Peres, H. Nunokawa and H. Minakata, *Constraining visible neutrino decay at KamLAND and JUNO*, *Eur. Phys. J. C* **80** (2020) 999 [[2002.12134](#)].
- [24] J. M. Berryman, A. de Gouvea and D. Hernandez, *Solar Neutrinos and the Decaying Neutrino Hypothesis*, *Phys. Rev. D* **92** (2015) 073003 [[1411.0308](#)].
- [25] M. Masud, P. Mehta, C. A. Ternes and M. Tortola, *Non-standard neutrino oscillations: perspective from unitarity triangles*, *JHEP* **05** (2021) 171 [[2103.11143](#)].
- [26] M. Chaves and T. Schwetz, *Resolving the LMA-dark NSI degeneracy with coherent neutrino-nucleus scattering*, *JHEP* **05** (2021) 042 [[2102.11981](#)].
- [27] A. Kumar, A. Khatun, S. K. Agarwalla and A. Dighe, *A New Approach to Probe Non-Standard Interactions in Atmospheric Neutrino Experiments*, *JHEP* **04** (2021) 159 [[2101.02607](#)].
- [28] S. S. Chatterjee and A. Palazzo, *Nonstandard Neutrino Interactions as a Solution to the $NO\nu A$ and $T2K$ Discrepancy*, *Phys. Rev. Lett.* **126** (2021) 051802 [[2008.04161](#)].
- [29] P. B. Denton, J. Gehrlein and R. Pestes, *CP -Violating Neutrino Nonstandard Interactions in Long-Baseline-Accelerator Data*, *Phys. Rev. Lett.* **126** (2021) 051801 [[2008.01110](#)].

- [30] K. S. Babu, D. Gonçalves, S. Jana and P. A. N. Machado, *Neutrino Non-Standard Interactions: Complementarity Between LHC and Oscillation Experiments*, *Phys. Lett. B* **815** (2021) 136131 [2003.03383].
- [31] P. Coloma, I. Esteban, M. C. Gonzalez-Garcia and M. Maltoni, *Improved global fit to Non-Standard neutrino Interactions using COHERENT energy and timing data*, *JHEP* **02** (2020) 023 [1911.09109].
- [32] I. Esteban, M. C. Gonzalez-Garcia and M. Maltoni, *On the Determination of Leptonic CP Violation and Neutrino Mass Ordering in Presence of Non-Standard Interactions: Present Status*, *JHEP* **06** (2019) 055 [1905.05203].
- [33] S.-F. Ge and S. J. Parke, *Scalar Nonstandard Interactions in Neutrino Oscillation*, *Phys. Rev. Lett.* **122** (2019) 211801 [1812.08376].
- [34] I. Esteban, M. C. Gonzalez-Garcia, M. Maltoni, I. Martinez-Soler and J. Salvado, *Updated constraints on non-standard interactions from global analysis of oscillation data*, *JHEP* **08** (2018) 180 [1805.04530].
- [35] P. B. Denton, Y. Farzan and I. M. Shoemaker, *Testing large non-standard neutrino interactions with arbitrary mediator mass after COHERENT data*, *JHEP* **07** (2018) 037 [1804.03660].
- [36] P. Langacker and D. London, *Lepton Number Violation and Massless Nonorthogonal Neutrinos*, *Phys. Rev. D* **38** (1988) 907.
- [37] S. Antusch, C. Biggio, E. Fernandez-Martinez, M. B. Gavela and J. Lopez-Pavon, *Unitarity of the Leptonic Mixing Matrix*, *JHEP* **10** (2006) 084 [hep-ph/0607020].
- [38] E. Fernandez-Martinez, M. B. Gavela, J. Lopez-Pavon and O. Yasuda, *CP-violation from non-unitary leptonic mixing*, *Phys. Lett. B* **649** (2007) 427 [hep-ph/0703098].
- [39] J. Kopp, M. Lindner, T. Ota and J. Sato, *Non-standard neutrino interactions in reactor and superbeam experiments*, *Phys. Rev. D* **77** (2008) 013007 [0708.0152].
- [40] W. Rodejohann, *On Non-Unitary Lepton Mixing and Neutrino Mass Observables*, *Phys. Lett. B* **684** (2010) 40 [0912.3388].
- [41] T. Ohlsson, *Status of non-standard neutrino interactions*, *Rept. Prog. Phys.* **76** (2013) 044201 [1209.2710].
- [42] M. M. Guzzo, P. C. de Holanda, O. L. G. Peres and E. M. Zavanin, *Stochastic Neutrino Mixing Mechanism*, *Phys. Rev. D* **87** (2013) 093003 [1304.5253].
- [43] S. K. Agarwalla, P. Bagchi, D. V. Forero and M. Tórtola, *Probing Non-Standard Interactions at Daya Bay*, *JHEP* **07** (2015) 060 [1412.1064].
- [44] F. J. Escrivuela Ferrándiz, *Phenomenology of non-standard neutrino interactions*, Ph.D. thesis, U. Valencia (main), 2016. Available at <https://roderic.uv.es/bitstream/handle/10550/50268/Escrivuela.Thesis.pdf?sequence=1>.
- [45] A. Falkowski, M. González-Alonso and Z. Tabrizi, *Consistent QFT description of non-standard neutrino interactions*, *JHEP* **11** (2020) 048 [1910.02971].
- [46] S. A. R. Ellis, K. J. Kelly and S. W. Li, *Leptonic Unitarity Triangles*, *Phys. Rev. D* **102** (2020) 115027 [2004.13719].
- [47] A. Falkowski, M. Gonzalez-Alonso and Z. Tabrizi, *Reactor neutrino oscillations as constraints on Effective Field Theory*, *JHEP* **05** (2019) 173 [1901.04553].

- [48] Y. Du, H.-L. Li, J. Tang, S. Vihonen and J.-H. Yu, *Non-standard interactions in SMEFT confronted with terrestrial neutrino experiments*, *JHEP* **03** (2021) 019 [[2011.14292](#)].
- [49] B. Pontecorvo, *Neutrino Experiments and the Problem of Conservation of Leptonic Charge*, *Sov. Phys. JETP* **26** (1968) 984.
- [50] Z. Maki, M. Nakagawa and S. Sakata, *Remarks on the Unified Model of Elementary Particles*, *Progress of Theoretical Physics* **28** (1962) 870.
- [51] P. Coloma and T. Schwetz, *Generalized mass ordering degeneracy in neutrino oscillation experiments*, *Phys. Rev.* **D94** (2016) 055005 [[1604.05772](#)].
- [52] M. González-Alonso, O. Naviliat-Cuncic and N. Severijns, *New physics searches in nuclear and neutron β decay*, *Prog. Part. Nucl. Phys.* **104** (2019) 165 [[1803.08732](#)].
- [53] T. Bhattacharya, V. Cirigliano, S. Cohen, R. Gupta, H.-W. Lin and B. Yoon, *Axial, Scalar and Tensor Charges of the Nucleon from 2+1+1-flavor Lattice QCD*, *Phys. Rev. D* **94** (2016) 054508 [[1606.07049](#)].
- [54] M. González-Alonso and J. Martin Camalich, *Isospin breaking in the nucleon mass and the sensitivity of β decays to new physics*, *Phys. Rev. Lett.* **112** (2014) 042501 [[1309.4434](#)].
- [55] C. Jarlskog, *Commutator of the Quark Mass Matrices in the Standard Electroweak Model and a Measure of Maximal CP Violation*, *Phys. Rev. Lett.* **55** (1985) 1039.
- [56] J. M. Berryman and P. Huber, *Sterile Neutrinos and the Global Reactor Antineutrino Dataset*, *JHEP* **01** (2021) 167 [[2005.01756](#)].
- [57] M. Estienne et al., *Updated Summation Model: An Improved Agreement with the Daya Bay Antineutrino Fluxes*, *Phys. Rev. Lett.* **123** (2019) 022502 [[1904.09358](#)].
- [58] KAMLAND collaboration, F. Suekane, *KamLAND*, *Prog. Part. Nucl. Phys.* **57** (2006) 106.
- [59] P. Vogel and J. F. Beacom, *Angular distribution of neutron inverse beta decay, $\bar{\nu}_e + p \rightarrow e^+ + n$* , *Phys. Rev. D* **60** (1999) 053003 [[hep-ph/9903554](#)].
- [60] P. Huber, J. Kopp, M. Lindner, A. Merle, W. Rodejohann, M. Rolinec et al., *Physics potential of future reactor neutrino experiments*, *Nuclear Physics B - Proceedings Supplements* **221** (2011) 360.
- [61] P. Huber, J. Kopp, M. Lindner, M. Rolinec and W. Winter, *New features in the simulation of neutrino oscillation experiments with GLoBES 3.0: General Long Baseline Experiment Simulator*, *Comput. Phys. Commun.* **177** (2007) 432 [[hep-ph/0701187](#)].
- [62] P. C. de Holanda, *Possible scenario for MaVaNs as the only neutrino flavor conversion mechanism in the Sun*, *JCAP* **0907** (2009) 024 [[0811.0567](#)].
- [63] P. C. de Holanda and A. Yu. Smirnov, *Solar neutrinos: The SNO salt phase results and physics of conversion*, *Astropart. Phys.* **21** (2004) 287 [[hep-ph/0309299](#)].
- [64] M. Maltoni and T. Schwetz, *Testing the statistical compatibility of independent data sets*, *Phys. Rev. D* **68** (2003) 033020 [[hep-ph/0304176](#)].
- [65] H. Pérez R, P. Kielanowski and S. R. Juárez W, *Cabibbo-Kobayashi-Maskawa matrix: rephasing invariants and parameterizations*, [1209.5812](#).
- [66] U. Sarkar and S. K. Singh, *CP violation in neutrino mass matrix*, *Nucl. Phys. B* **771** (2007) 28 [[hep-ph/0608030](#)].

A Analytical expressions

After a straightforward calculation, we find the $N^{\text{non-osc}}$, N^{osc} , and N^{CP} terms in each oscillation scale (Δm_{21}^2 and Δm_{3i}^2) and for different NSI couplings each time ($[\tilde{\epsilon}_X]_{e\mu}$ and $[\tilde{\epsilon}_X]_{e\tau}$). We will not consider mixing terms like $[\tilde{\epsilon}_X]_{e\tau}[\tilde{\epsilon}_X]_{e\mu}$, therefore our analysis is focused on the effects of the effective parameters.

First, we present the non-oscillation terms, the term will be the same for any parameter, and they do not depend on the oscillation scale. They can appear for example, in beta decays or reactor short baseline experiments:

$$N^{\text{non-osc}} = 1 + 2 |[\tilde{\epsilon}_X]_{e\alpha}|^2 d_{\text{XL}} p_{\text{XL}} + |[\tilde{\epsilon}_X]_{e\alpha}|^4 d_{\text{XX}} p_{\text{XX}}, \quad (\text{A.1})$$

where α can be μ or τ . We point that those terms appears always as higher than quadratic order on the ϵ .

Secondly, we present the atmospheric scale terms, that is, the terms that follow the Δm_{3i}^2 . Using the approximation where $\Delta m_{32}^2 \approx \Delta m_{32}^2$, we found:

Atmospheric scale: $\tilde{\epsilon}_{e\mu}$

$$N_{\text{atm}}^{\text{osc}} = s_{2\theta_{13}}^2 + 4s_{13} |[\tilde{\epsilon}_X]_{e\mu}|^2 d_{\text{XL}} p_{\text{XL}} \quad (\text{A.2})$$

$$N_{\text{atm}}^{\text{osc-CP}} = 0 \quad (\text{A.3})$$

Atmospheric scale: $\tilde{\epsilon}_{e\tau}$

$$\begin{aligned} N_{\text{atm}}^{\text{osc}} = & s_{4\theta_{13}} \text{Re}\{[\tilde{\epsilon}_X]_{e\tau}\} (d_{\text{XL}} + p_{\text{XL}}) + s_{2\theta_{13}}^2 + 4 \left(|[\tilde{\epsilon}_X]_{e\tau}|^2 - \text{Re}\{[\tilde{\epsilon}_X]_{e\tau}\}^2 s_{2\theta_{13}}^2 \right) d_{\text{XL}} p_{\text{XL}} \\ & - |[\tilde{\epsilon}_X]_{e\tau}|^2 s_{2\theta_{13}}^2 (d_{\text{XX}} + p_{\text{XX}}) - |[\tilde{\epsilon}_X]_{e\tau}|^2 s_{4\theta_{13}}^2 \text{Re}\{[\tilde{\epsilon}_X]_{e\tau}\} (d_{\text{XX}} p_{\text{XL}} + p_{\text{XX}} d_{\text{XL}}) \\ & + |[\tilde{\epsilon}_X]_{e\tau}|^4 d_{\text{XX}} p_{\text{XX}} s_{2\theta_{13}}^2 \end{aligned} \quad (\text{A.4})$$

$$\begin{aligned} N_{\text{atm}}^{\text{CP}} = & + \text{Im}\{[\tilde{\epsilon}_X]_{e\tau}\} (d_{\text{XL}} - p_{\text{XL}}) s_{2\theta_{13}} \\ & + |[\tilde{\epsilon}_X]_{e\tau}|^2 \text{Im}\{[\tilde{\epsilon}_X]_{e\tau}\} (d_{\text{XX}} p_{\text{XL}} - d_{\text{XL}} p_{\text{XX}}) s_{2\theta_{13}}^2 \end{aligned} \quad (\text{A.5})$$

As can be seen from Eq. (A.5), CP violation term appears only for the $e\tau$ parameter. We also expect that, if the coupling is small, the $e\tau$ parameters are more important in the atmospheric scale than the $e\mu$. This comes from the fact that the $e\tau$ appears at linear order, opposite to $e\mu$ that appears only at quadratic.

Next, we will present the behavior of the atmospheric scale in the case we break the mass hierarchy, that is, when we can consider $\Delta m_{32}^2 \neq \Delta m_{32}^2$. The effects of breaking the hierarchy have similar effects in the $e\tau$ parameter as they have in the standard oscillation case:

$$N_{32}^{\text{osc}} = N_{\text{atm}}^{\text{osc}} s_{12}^2, \quad N_{31}^{\text{osc}} = N_{\text{atm}}^{\text{osc}} c_{\theta_{12}}^2, \quad (\text{A.6})$$

$$N_{32}^{\text{CP}} = N_{\text{atm}}^{\text{CP}} s_{12}^2, \quad N_{31}^{\text{CP}} = N_{\text{atm}}^{\text{CP}} c_{\theta_{12}}^2. \quad (\text{A.7})$$

In contrast, for the $e\mu$ parameter, we have more complex changes:

$$N_{32}^{\text{osc}} = s_{2\theta_{13}}^2 s_{12}^2 + \text{Re}\{[\tilde{\epsilon}_X]_{e\mu}\} c_{13} (p_{\text{XL}} + d_{\text{XL}}) s_{2\theta_{12}} s_{13}^2 + 4s_{13} c_{12}^2 |[\tilde{\epsilon}_X]_{e\mu}|^2 d_{\text{XL}} p_{\text{XL}} \quad (\text{A.8})$$

$$N_{32}^{\text{CP}} = - \text{Im}\{[\tilde{\epsilon}_X]_{e\mu}\} c_{13} (p_{\text{XL}} - d_{\text{XL}}) s_{2\theta_{12}} s_{13}^4, \quad (\text{A.9})$$

$$N_{31}^{\text{osc}} = s_{2\theta_{13}}^2 c_{12}^2 - \text{Re}\{[\tilde{\epsilon}_X]_{e\mu}\} c_{13}(p_{\text{XL}} + d_{\text{XL}}) s_{2\theta_{12}} s_{13}^2 + 4s_{13} s_{12}^2 |[\tilde{\epsilon}_X]_{e\mu}|^2 d_{\text{XL}} p_{\text{XL}} \quad (\text{A.10})$$

$$N_{31}^{\text{CP}} = + \text{Im}\{[\tilde{\epsilon}_X]_{e\mu}\} c_{13}(p_{\text{XL}} - d_{\text{XL}}) s_{2\theta_{12}} s_{13}^4 \quad (\text{A.11})$$

We expect that the $e\mu$ non-standard hierarchy terms Eqs. (A.8), (A.9), (A.10), and (A.11) to be approximated similar to the standard and $e\tau$ case if we neglect the $s_{\theta_{13}}$ quadratic terms, leading to: $N_{32}^{\text{osc}} \approx N_{\text{atm}}^{\text{osc}} s_{\theta_{12}}^2$, $N_{31}^{\text{osc}} \approx N_{\text{atm}}^{\text{osc}} c_{\theta_{12}}^2$ and $N_{32}^{\text{osc-CP}} \approx 0$.

Finally, we present the rates for the solar scale, that is, terms that are proportional to Δm_{21}^2 :

Solar scale: $\tilde{\epsilon}_{e\mu}$

$$\begin{aligned} N_{\text{Sun}}^{\text{osc}} = & c_{13}^4 s_{2\theta_{12}}^2 - \text{Re}\{[\tilde{\epsilon}_X]_{e\mu}\} c_{13}^3 s_{4\theta_{12}} (d_{\text{XL}} + p_{\text{XL}}) \\ & + \left(|[\tilde{\epsilon}_X]_{e\mu}|^2 + \text{Re}\{[\tilde{\epsilon}_X]_{e\mu}\}^2 s_{2\theta_{12}}^2 \right) 4c_{13}^2 d_{\text{XL}} p_{\text{XL}} - |[\tilde{\epsilon}_X]_{e\mu}|^2 s_{2\theta_{12}}^2 (d_{\text{XX}} + p_{\text{XX}}) \\ & - |[\tilde{\epsilon}_X]_{e\mu}|^2 \text{Re}\{[\tilde{\epsilon}_X]_{e\mu}\} c_{13} s_{4\theta_{12}} (d_{\text{XX}} p_{\text{XL}} + p_{\text{XX}} d_{\text{XL}}) + |[\tilde{\epsilon}_X]_{e\mu}|^4 s_{2\theta_{12}}^2 d_{\text{XX}} p_{\text{XX}} \end{aligned} \quad (\text{A.12})$$

$$N_{\text{Sun}}^{\text{CP}} = + \left[c_{13}^2 (d_{\text{XL}} - p_{\text{XL}}) + |[\tilde{\epsilon}_X]_{e\mu}|^2 (d_{\text{XX}} p_{\text{XL}} - d_{\text{XL}} p_{\text{XX}}) \right] \text{Im}\{[\tilde{\epsilon}_X]_{e\mu}\} c_{13} s_{2\theta_{12}} \quad (\text{A.13})$$

Solar scale: $\tilde{\epsilon}_{e\tau}$

$$\begin{aligned} N_{\text{Sun}}^{\text{osc}} = & c_{13}^4 s_{2\theta_{12}}^2 - 2s_{13} c_{13}^3 \text{Re}\{[\tilde{\epsilon}_X]_{e\tau}\} (d_{\text{XL}} + p_{\text{XL}}) s_{2\theta_{12}}^2 \\ & + s_{2\theta_{13}}^2 s_{2\theta_{12}}^2 \text{Re}\{[\tilde{\epsilon}_X]_{e\tau}\}^2 d_{\text{XL}} p_{\text{XL}} + \frac{1}{4} |[\tilde{\epsilon}_X]_{e\tau}|^2 s_{2\theta_{12}}^2 s_{2\theta_{13}}^2 (d_{\text{XX}} + p_{\text{XX}}) \\ & - c_{13} s_{13}^3 |[\tilde{\epsilon}_X]_{e\tau}|^2 s_{4\theta_{12}}^2 \text{Re}\{[\tilde{\epsilon}_X]_{e\tau}\} (d_{\text{XX}} p_{\text{XL}} + p_{\text{XX}} d_{\text{XL}}) \\ & + s_{13}^4 |[\tilde{\epsilon}_X]_{e\tau}|^4 d_{\text{XX}} p_{\text{XX}} s_{2\theta_{12}}^2 \end{aligned} \quad (\text{A.14})$$

$$N_{\text{Sun}}^{\text{osc-CP}} = 0. \quad (\text{A.15})$$

B Rephasing invariants with non-standard neutrino interaction

In standard oscillation induced by PMNS mixing matrix there are invariants by phase rephasing [65] called Jaroskog invariants [55]. We follow Ref. ([66]) to construct the invariants by global phase rephasing for our BSM Lagrangian. If we made global rephasing the particle fields

$$\begin{aligned} \nu_i & \rightarrow e^{i\delta_i} \nu_i & l_\alpha & \rightarrow e^{i\eta_\alpha} l_\alpha \\ u & \rightarrow e^{i\delta_u} u & d & \rightarrow e^{i\delta_d} d \end{aligned}$$

then the Lagrangian given in Eq. (1.1) it will invariant if

$$\begin{aligned} V_{ud} & \rightarrow V_{ud} e^{i(\delta_u - \delta_d)} & U_{\alpha j} & \rightarrow U_{\alpha j} e^{i(\eta_\alpha - \delta_j)} \\ (\epsilon_S)_{\alpha\beta} & \rightarrow (\epsilon_S)_{\alpha\beta} e^{+i(\eta_\alpha - \eta_\beta)} & (\epsilon_T)_{\alpha\beta} & \rightarrow (\epsilon_T)_{\alpha\beta} e^{+i(\eta_\alpha - \eta_\beta)} \end{aligned}$$

Now, with these rules we can apply to the with NSIpd rate (2.15) and we have found that the each term of the rate is invariant by these global rephasing.

C Solar+KamLand analysis

Here we present the Solar+KamLand analysis using the χ_{KL}^2 and the χ_{SUN}^2 . The results of the 1D and 2D χ^2 functions are shown in fig. 7. For the scalar interactions, there is no substantial differences with the standard oscillation. However, in the tensor case, there is an improvement of around 1.3σ in the statistics compared to the standard model.

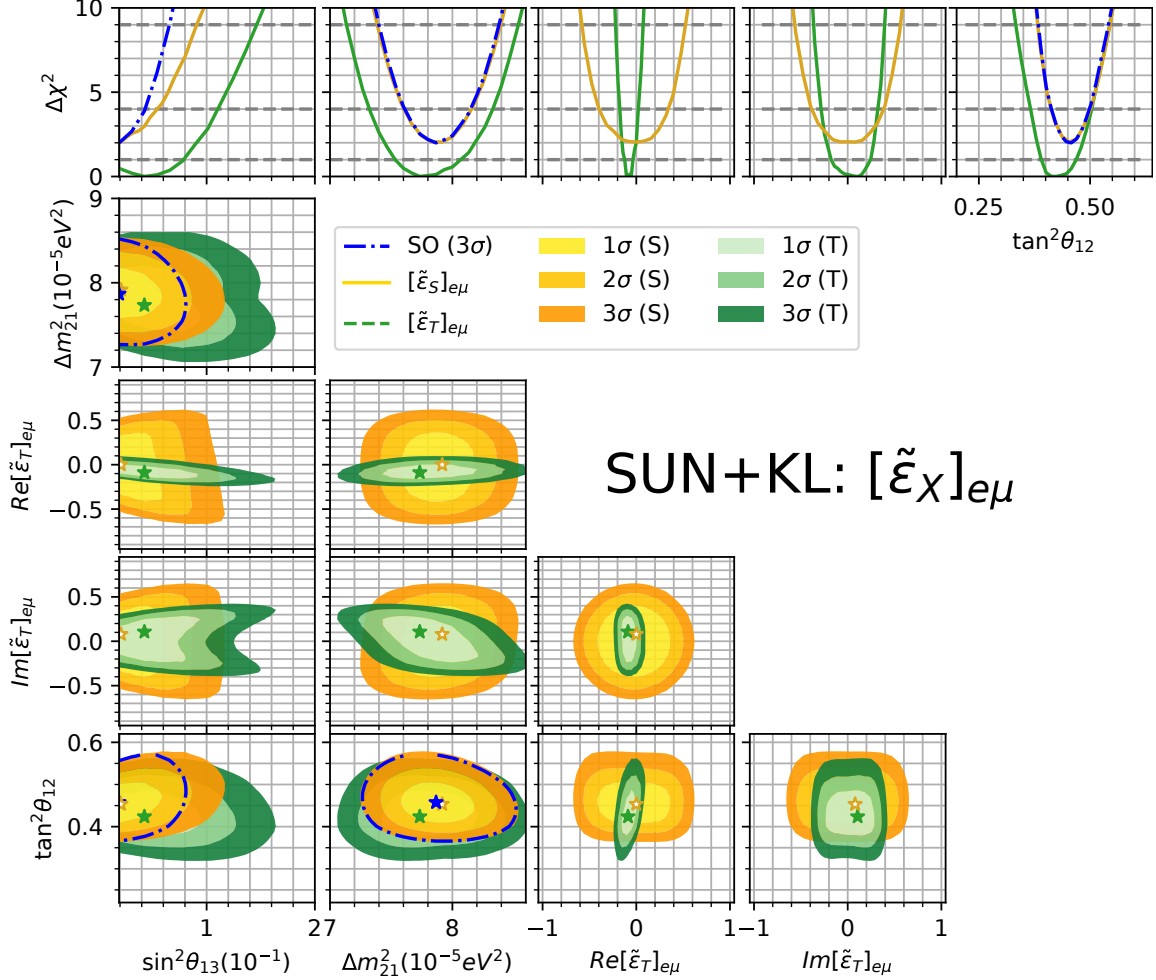


Figure 7. The $\Delta\chi^2$ of Kamland combined with solar experiments in the presence of $[\tilde{\xi}_X]_{e\tau}$, the contour levels at 1σ , 2σ and 3σ and the 1D χ^2 curves. In green (yellow) is the NSI tensor (scalar) case and in dash-dotted blue is $\chi_{\text{SO}}^2 - \min(\chi_{\text{NSI}}^2)$.